

Tunable bulk photovoltaic effect in strained γ -GeSe

Hong-Guk Min,^{*} Churlhi Lyi^{✉,*} and Youngkuk Kim^{✉†}

Department of Physics, Sungkyunkwan University, Suwon 16419, Korea

 (Received 13 March 2022; revised 13 November 2022; accepted 15 November 2022; published 30 November 2022)

Recently, Lee *et al.* [*Nano Lett.* **21**, 4305 (2021)] synthesized the monochalcogenide GeSe in a polar phase, referred to as the γ -phase. Motivated by this work, we study the shift current of γ -GeSe and its tunability via an in-plane uniaxial strain. Using first-principles calculations, we uncover the electronic structure of strained γ -GeSe systems. We then calculate the frequency-dependent shift current conductivities at various strains. The tunability increases the shift current to $\sim 40 \mu\text{A}/\text{V}^2$ for visible light. Moreover, the direction of the shift current can be inverted by a light strain. Markedly, noticeable behavior is found in the zero-frequency limit, which can be indicative of band inversion and electronic phase transition driven by the strain. Our results suggest that the shift current can be tangible proof of bulk electronic states of γ -GeSe.

DOI: [10.1103/PhysRevB.106.205153](https://doi.org/10.1103/PhysRevB.106.205153)

I. INTRODUCTION

A dramatic consequence of quantum mechanics featured in light-matter interaction is the generation of photovoltaic current without frequency dependence under light illumination. An electric field $E(\omega)$ with angular frequency ω can drive a second-order nonlinear response of electrons that leads to a direct current,

$$J_a = \sum_{bc} \sigma_{abc} E^b(\omega) E^c(-\omega), \quad (1)$$

referred to as the shift current [1–5]. Here, σ_{abc} is a shift current conductivity tensor, and a , b , and c represent coordinate indices. Since the early discovery in the 1970s [6–8], the bulk photovoltaic effect has attracted much attention due to its potential applications in solar cells. Bulk photovoltaic effects can generally arise from diverse intra- and interband processes, including the shift current, injection current, nonlinear Hall effect, and second-order jerk current [9]. Notably, the shift current has attracted renewed attention [10–12] due to its connection to band topology, allowing for design principles for high efficiency of light conversion beyond the Shockley-Queisser limit of conventional p - n junctions [13]. This has enabled exciting discoveries of bulk photovoltaic materials, including many oxides [14–17], quantum wells [18,19], semiconductors [20–23], organic crystals [24,25], nanostructures [26–31], and two-dimensional systems [32–34].

Along with the recent developments of topological states of matter [35,36], the shift current has attracted renewed attention in view of band topology. It turns out that the excited electrons can probe the topology and geometry of the conduction and valence bands [32,37–40]. This picture explains the generation of shift current as being due to the change in electronic polarizations during the band transition of electrons

dressed by photons [38]. The relationship between polarization and the shift current of electrons is further demonstrated in monochalcogenide monolayers [32,34], in which optimized polarization magnifies the shift current up to $\sim 100 \mu\text{A}/\text{V}^2$. Despite these outstanding explorations, topological aspects of shift current have remained largely unexplored to date, partly due to the lack of suitable topological platforms. Encouragingly, a recent experiment reported the synthesis of a new polar monochalcogenide system, GeSe [41,42], providing an opportunity to explore the shift current phenomena.

In this paper, we perform first-principles calculations to study the shift current response of strained γ -GeSe. We calculate the shift current conductivity tensors for various in-plane uniaxial tensile strains. We show that the shift current of γ -GeSe is highly tunable in magnitude and direction within 5% tensile strain. In particular, a significant enhancement is expected in a high-frequency, near-visible-light regime, captured in, for example, the σ_{zxx} component of the shift current conductivity tensor. In addition, a noticeable change in the shift current is found from, for example, σ_{zyy} and σ_{zxx} near zero frequency. Electronic energy bands and the density of states are calculated to explain these behaviors. We attribute the strain sensitivity of the shift current to band inversion captured in the changes in orbital characters.

II. COMPUTATION DETAILS

Our first-principles calculations were performed based on density functional theory (DFT) as implemented in the QUANTUM ESPRESSO package [43]. We employed the fully relativistic atomic pseudopotentials provided in the PSEUDODOJO library [44]. The employed pseudopotentials were built using the norm-conserving optimized Vanderbilt pseudopotential scheme [45]. To describe the exchange-correlation energies, we used the Perdew-Burke-Ernzerhof generalized gradient approximation [46]. The plane wave basis was generated under a kinetic energy cutoff of 100 Ry. Self-consistent fields were achieved by employing the Monkhorst-Pack sampling of \mathbf{k}

^{*}These authors contributed equally to this work.

[†]youngkuk@skku.edu

points from the $13 \times 13 \times 3$ grid of the first Brillouin zone (BZ) [47]. The crystal structure of pristine γ -GeSe is fully relaxed with the $13 \times 13 \times 3$ Monkhorst-Pack k grid until the total force is fully converged below 10^{-4} Ry/bohr. The fully relaxed lattice constants were calculated as $a \simeq 3.76$ Å and $c \simeq 15.39$ Å, which are in good agreement with the experiment [41]. Under strain, we fixed the lattice constant only along the strained axis and relaxed the internal atomic coordinates and the other cell parameters. To calculate shift current, we used the Wannier-interpolation scheme [48]. The Wannier Hamiltonians were first generated using the WANNIER90 package [48,49]. To obtain an initial guess for the projection functions, we used the unified method for Wannier localization [50,51]. These Wannier Hamiltonians well reproduced the DFT bands for $E < 10$ eV with respect to the Fermi level $E = 0$ eV. Using the constructed Wannier Hamiltonians, we calculated the shift current conductivity tensors using the POSTW90 package [48]. The shift current conductivity tensors were calculated on the uniform $100 \times 100 \times 25$ k grid of the BZ. The \mathbb{Z}_2 topological invariants [52,53] on time-reversal-invariant planes and mirror Chern numbers [54,55] on a g_y -invariant plane $k_y = 0$ were evaluated from the Wannier center flows [56] as implemented in WANNIERTOOLS [57].

III. RESULTS AND DISCUSSION

A. Atomic structures and symmetries

We begin by delineating the atomic structure and symmetries of γ -GeSe. As illustrated in Fig. 1, the unit cell of pristine γ -GeSe comprises eight atoms with four formula units. Each atom constitutes a distinct triangular sublattice layer, leading to eight vertically stacked sublattices. The layered structure comprises two quadruple layers: B - C - A - B and C - B - A - C layers occupied Se-Ge-Ge-Se and Se-Ge-Ge-Se atoms, respectively [see Fig. 1(b)]. The hexagonal BZ and corresponding high-symmetry k points of pristine γ -GeSe are shown in Fig. 1(c). The pristine atomic structure preserves the hexagonal space group symmetries of $P6_3mc$ (No. 186), which is generated by the mirror M_{xy} and sixfold screw $S_{6z} = \{C_{6z}|00\frac{1}{2}\}$. Here, C_{6z} is a sixfold rotation with respect to the z axis, and $\{00\frac{1}{2}\}$ represents translation by half of the out-of-plane (z -directional) unit vector. Spatial inversion is absent in $P6_3mc$ (No. 186), which is required to generate the shift current.

To reduce the crystalline symmetries, which can render qualitative changes in the electronic structure of γ -GeSe and, correspondingly, the shift current response, we consider a uniaxial tensile strain ϵ , applied along the (110) armchair direction. As illustrated in Fig. 1(a), the uniaxial tensile strain ϵ is defined as $\epsilon = \frac{l_y - \sqrt{3}a}{\sqrt{3}a} \times 100\%$, where l_y is the stretched length of the unit cell along the y direction. It is evident that the applied strain lowers the sixfold screw symmetry $S_{6z} = \{C_{6z}|00\frac{1}{2}\}$ of the pristine structure into $S_{2z} = \{C_{2z}|00\frac{1}{2}\}$ of the strained one. Here, C_{2z} is a twofold rotation with respect to the z axis. As a result, the strained γ -GeSe structure preserves the crystalline symmetries of the orthorhombic $Cmc2_1$ (No. 36) space group, generated by a glide mirror $g_y = \{M_y|00\frac{1}{2}\}$ and the twofold screw S_{2z} . The corresponding BZ and the high-symmetry k points are depicted in Fig. 1(d). We note that the presence of the mirror M_x and the glide g_y is crucial to nullify

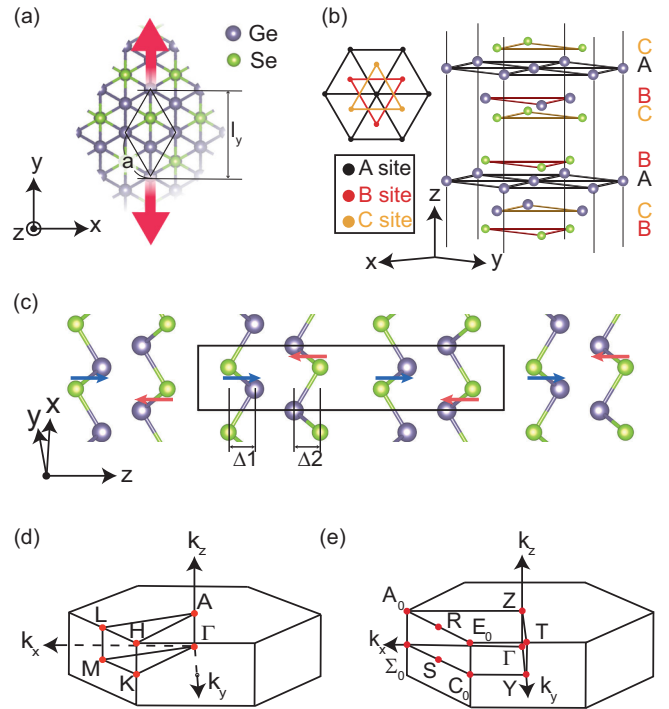


FIG. 1. Crystal structure and the Brillouin zone (BZ) of γ -GeSe. (a) Top view of the pristine γ -GeSe atomic structure. Red arrows indicate the direction of uniaxial strain. (b) Lateral view of pristine γ -GeSe. The A, B, and C triangular sublattices in each Ge-Se honeycomb layer are indicated by black, red, and yellow color schemes, respectively. (c) Side view of the pristine γ -GeSe atomic structure. A primitive unit cell is indicated by a black box. The buckling parameters Δ_1 and Δ_2 are introduced. The blue and red arrows indicate the polar direction of each layer. (d) Hexagonal BZ and high-symmetry points of pristine γ -GeSe. (e) Orthorhombic BZ and corresponding high-symmetry points of strained γ -GeSe.

the in-plane polarity in the strained system. By contrast, the out-of-plane polarization is allowed, attributed to the breaking of coplanar mirror symmetry by the buckling of the Ge and Se sublattice in each Ge-Se layer. We find that applying tensile strains up to 5% reduces the buckling parameters Δ_1 and Δ_2 by 3%. Therefore, strains may significantly affect the buckling, which can be considered a polar distortion, which is necessary to produce the shift current response.

B. Electronic structures

1. Band structures

Before presenting the shift current calculations, let us first clarify the electronic structure of pristine and strained γ -GeSe. Figures 2(a)–2(d) show the band structures of the pristine and 3%, 4%, and 5% strained systems, respectively. A semimetallic nature is generically observed for the tested strains from the conduction and valence bands that overlap with the Fermi energy $E_F = 0$ eV. Correspondingly, electron and hole pockets appear near the high-symmetry Γ and M points, respectively. While the indirect gap is absent, a close inspection reveals that a direct band gap exists throughout the entire BZ, which allows for the shift current calculations. For example, in the pristine case [Fig. 2(a)], the minimum direct

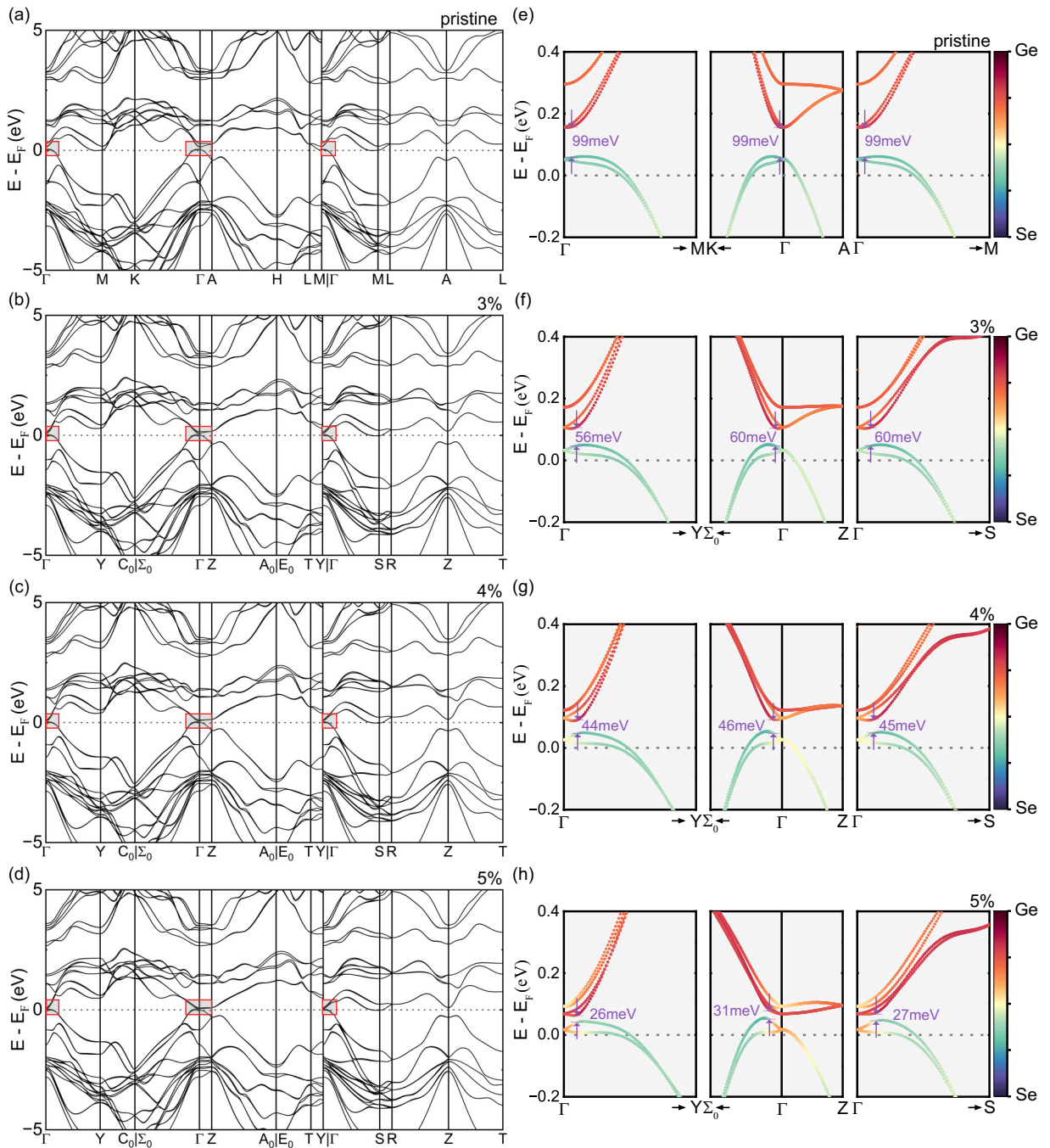


FIG. 2. The band structure of γ -GeSe under tensile uniaxial strain. (a)–(d) Energy bands of the pristine and 3%, 4%, and 5% strained systems. (e)–(h) Magnified views of the boxed regions in the full energy bands of the pristine and 3%, 4%, and 5% strained systems. The color coding represents the Ge and Se $s + p$ orbitals.

band gap occurs in the vicinity of the Γ point, which is around 99 meV. Under a strain of up to 5%, the semimetallic nature becomes more prominent. The size of the electron and the hole pockets increases with an increased overlap with the Fermi energy, as shown in Figs. 2(a)–2(d). The minimum direct band gap significantly decreases as the strain increases. From 0% to 5%, the minimum direct band gap is monotonically reduced from 99 to 26 meV [see Figs. 2(e)–2(f)].

The band inversion near the Γ point is evident from the orbital projected bands shown in Figs. 2(e)–2(h). For the pristine system, the valence and conduction bands mainly

comprise the sp^3 orbitals of Se and Ge, respectively. The majority orbital at Γ starts to alter near 4% strain, signaling an inversion between the conduction and valence bands. The Se and Ge sp^3 orbitals become larger in the 5% strained conduction and valence bands near Γ , respectively. The band inversion captured in the orbital-projected band structures is responsible for the abrupt changes in the shift current near the zero-frequency regime, as we will show later.

We observe from the calculated band structure that it captures the structural anisotropy of the layered system. The band structures on the $k_z = 0$ and $k_z = \pi$ planes resemble each

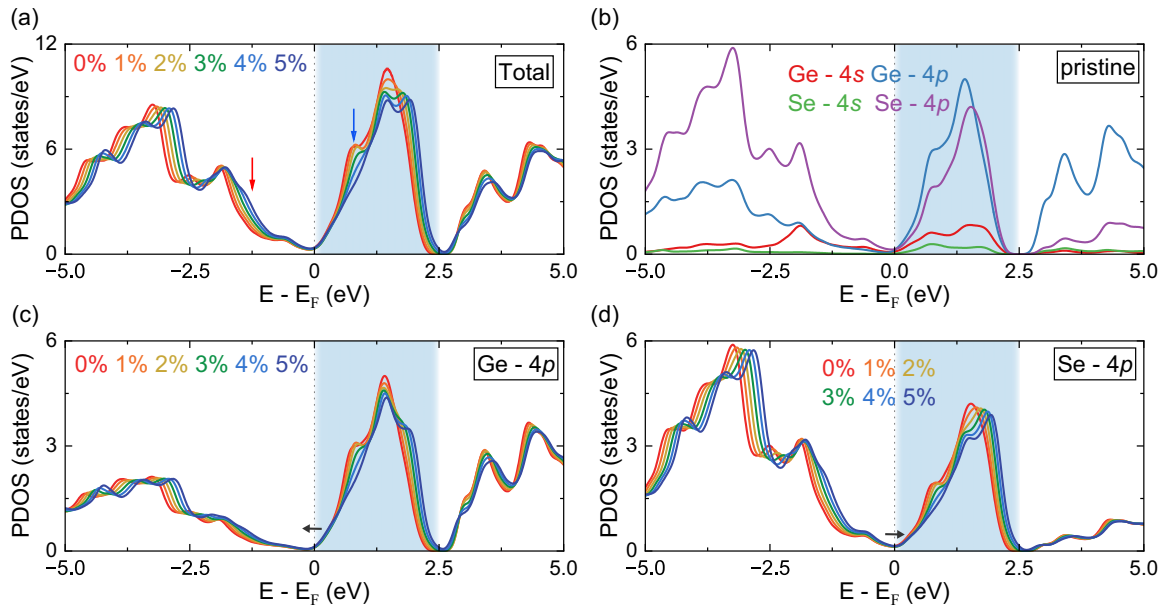


FIG. 3. The DOS and PDOS of γ -GeSe under tensile strain. (a) The total density of states, obtained with the sum of the projected density of states. The change in the total DOS is shown by increasing the tensile strain from 0% to 5%. The red and blue arrows indicate the peaks at -1.2 and 0.8 eV, respectively. (b) Density of states, projected on the $4s$ and $4p$ orbitals of Ge and Se atoms for the pristine case. (c)–(f) The change in each projected density of states from increasing the tensile strain from 0% to 5%. The black arrows indicate the direction of dip shifts with increasing strain. Blue boxes highlight the energy range of $0.0 < E < 2.5$ eV.

other. This manifests the van der Waals–type weak interlayer interaction. Similarly, dispersion along Γ -A is relatively weak. In addition, the valence bands exhibit a stronger dispersion than the rest of the bands, including the conduction bands. The enhanced dispersion of the valence bands can be attributed to the relatively stronger interlayer interaction within a quadruple layer than the inter-quadruple-layer interaction.

Noticeable changes are further found as follows. First, bands are less (more) dispersive along the parallel (normal) direction under strain. For example, the band dispersion is slightly increased (decreased) along the Y - C_0 (Γ - Y) direction. This captures the enhanced (dwindled) intralayer hopping of electrons under the in-plane uniaxial tensile strain, which shrinks the in-plane perpendicular (colinear) dimension and, correspondingly, the interlayer distances. In addition, the band degeneracy changes due to the reduced symmetries under strain. For example, the band crossings along the Γ -A line open a gap due to the absence of C_{3z} . The space group $P6_3mc$ (No. 186) of the pristine system has three different two-dimensional irreducible representations: Δ_7 , Δ_8 , and Δ_9 . In contrast, the $Cmc2_1$ (No. 36) space group of the strained system has only a single two-dimensional irreducible representation: Δ_5 . Thus, the band crossings are absent, and only anticrossings are present under strain along the high-symmetry Δ line.

2. Density of states

The changes in electronic structure are more apparent in the total density of states (DOS) and the orbital projected density of states (PDOS). Figure 3 shows the DFT DOS and PDOS. They signal the large shift current responses

of γ -GeSe associated with the quasi-two-dimensional nature of the layered structure. In detail, intensified peaks appear throughout the -5.0 to 5.0 eV energy range. For example, considerable DOSs are accumulated in the range $0.0 < E < 2.5$ eV, in line with the formation of weakly dispersing bands in this energy range. This again captures the quasi-two-dimensional nature of γ -GeSe. The PDOSs in Figs. 3(a)–3(d) show that these peaks consist of both Ge $4p$ and Se $4p$ orbitals. Close inspection reveals that the valence bands mainly comprise Se $4p$ orbitals, while the conduction bands consist of both Ge $4p$ and Se $4p$ orbitals.

Examining detailed changes in the total DOS driven by the strain, we observe the following. First, the peaks develop and are suppressed at $E \simeq -1.2$ eV [red arrow in Fig. 3(a)] and $E \simeq 0.8$ eV [blue arrow in Fig. 3(a)], respectively, as we gradually increase the strain from 0% to 5%. These trends are prominent in the PDOS of Ge and Se $4p$ orbitals. The suppression (development) of the peaks occurs at the conduction and valence bands due to the enhanced (weakened) hybridization of those orbitals by the strain. Second, there exists a blueshift of peaks and dips in the occupied energy regime, such as for $E \simeq -4.6$, -3.8 , -3.2 , and -2.8 eV. This matches well with the energy growth of the valence bands due to the tensile strain in Fig. 2. Similarly, a trend in blueshift appears when the strain suppresses the peaks of the conduction bands, as shown at $E \simeq 1.5$, 3.4 , and 4.3 eV. Finally, the Ge and Se $4p$ orbital characters are exchanged between the conduction and valence bands at the near-zero dips at $E \sim 0$ as band inversion occurs [see the black arrows in Figs. 3(c) and 3(d)]. This trend is in line with the sensible dependence of the shift current on the strain near zero energy, which we will discuss in detail in the next section.

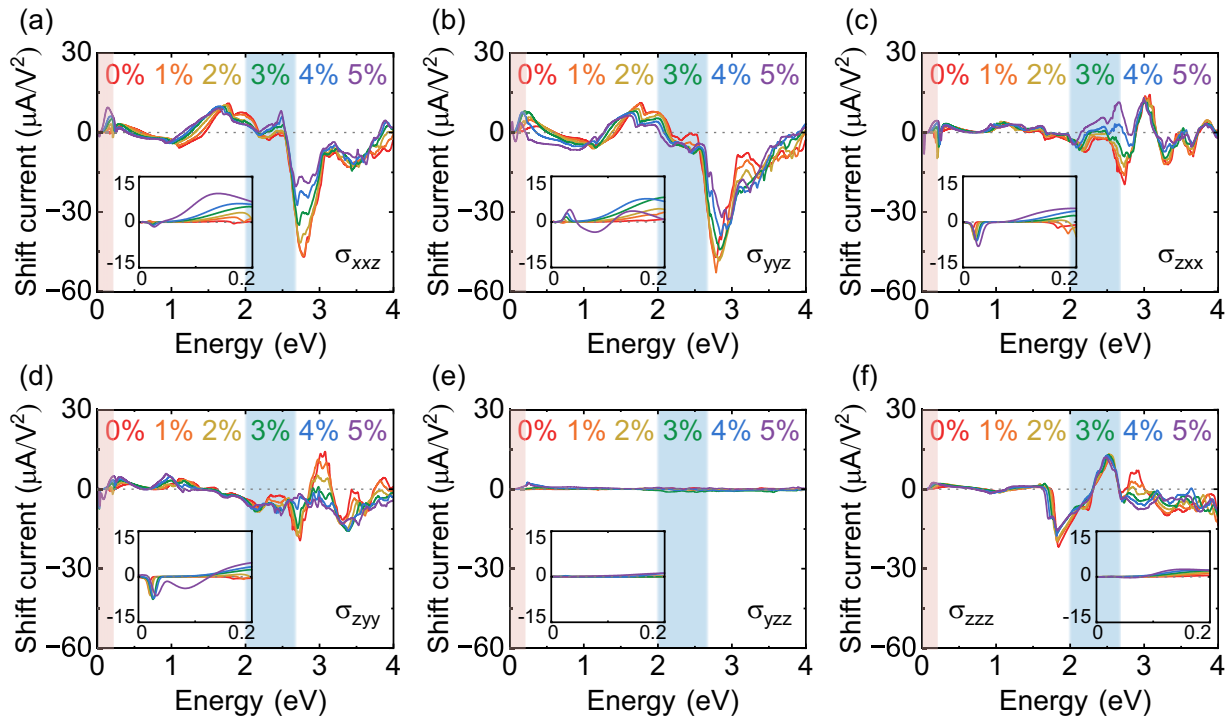


FIG. 4. Shift current conductivity tensors of γ -GeSe as a function of uniaxial tensile strains. Different color schemes are used for different strains from 0% to 5%. Blue boxes indicate the visible light regime from 2.0 to 2.7 eV. The red boxes highlight the energy regime near zero from 0 to 0.2 eV. The insets show a magnified view of the shift current for the 0 to 0.2 eV energies in the $\pm 15 \mu\text{A}/\text{V}^2$ shift current window.

C. Shift currents

Figure 4 shows the shift current conductivity tensors calculated using our first-principles methods. Our calculations produce a shift current conductivity σ_{abc} that is symmetric under the exchange of the b and c indices in both pristine and strained systems. This means that only 18 components become distinct in the components of the three-rank tensor. Out of these, only five components (σ_{zxx} , σ_{zyy} , σ_{zzz} , σ_{yyz} , σ_{xxz}) produce a non-negligible value, in good agreement with the symmetries of $P6_3mc$ ($Cmc2_1$) for pristine (strained) γ -GeSe [58]. Figure 4 shows the five nonvanishing components. In addition, as a representative example of a vanishing component, we show the calculation result for σ_{yzz} in Fig. 4(e), which has a negligible value.

We further find a trend exists in which those with an odd number of z indices have a relatively larger value than those with an even number of z indices. This also applies to the strained case, in which C_{3z} is broken. The rationale for saying that this trend is due to symmetry constraints is associated with the g_x and M_y symmetries. An even number of z components leads to an odd number of x or y indices. A nonzero value of these components infers that shift current can flow in a preferred direction indistinguishable by the system with g_x and M_y . Thus, these components have a negligible value. Similarly, a symmetry constraint arises that is associated with the C_{3z} symmetry manifested in the xxz (zxx) and yyz (zyy) components. They share a similar profile as a function of energy, as shown in Figs. 4(a) and 4(b) [Figs. 4(c) and 4(d)]. Under strain, these components start to deviate, manifesting the absence of C_{3z} symmetry.

Regarding the magnitude, we note that a considerable value for the shift current is expected from γ -GeSe up to $\sim 40 \mu\text{A}/\text{V}^2$ for visible light. This value exceeds those of the known shift current materials. For example, PbTiO_3 realized in a three-dimensional bulk has a maximum shift current conductivity tensor of $\sim 10 \mu\text{A}/\text{V}^2$; that of BaTiO_3 is $18 \mu\text{A}/\text{V}^2$, and that of SbSI is $15 \mu\text{A}/\text{V}^2$ [5,23,59].

The strain affects the shift current response not only in its magnitude but also in its direction. In particular, the zxx component exhibits the most prominent directional change in response to the strain near the visible light frequency range [$2.0 < E < 2.7$ eV; see Fig. 4(c)]. One can observe a sign change in the current due to strain in this wide energy range. This sign change is important in particular because it can be directly observed through the directional change in the current. Directional reversals are also observed in other components such as σ_{xxz} and σ_{yyz} , as shown in Figs. 4(a) and 4(b). We note that a directional reversal occurs within 4% strained. This is much more feasible than 5%, which induces band inversion. Such prominent changes in the shift current allow for an opportunity to engineer the direction of the photocurrent using the strain as a controllable knob.

Finally, the shift current conductivity exhibits marked strain dependence near zero-frequency fields. A few remarks and speculations are as follows. First, the yyz component is particularly enhanced with respect to the xxz component upon applying 4% strain, which is suppressed near zero frequency. Therefore, the occurrence of the y -directional component upon the exertion of an oblique incidence of a terahertz field can be used as proof of crystalline symmetries. While a similar

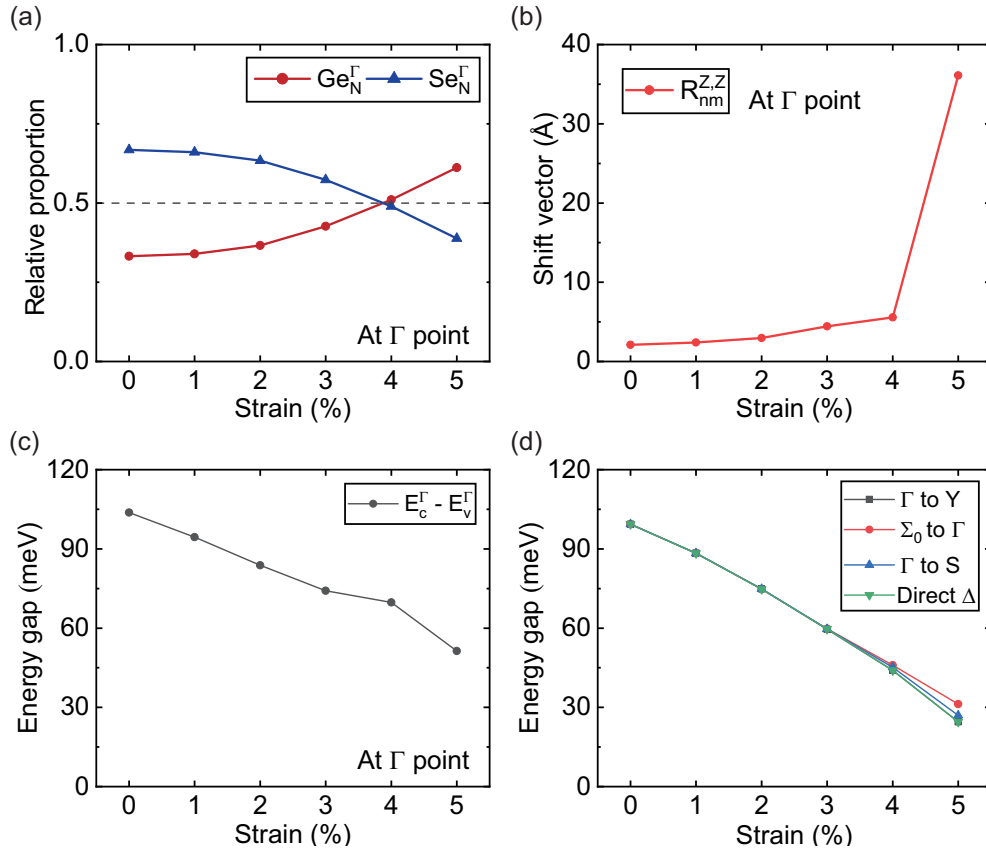


FIG. 5. (a) Relative proportion of Ge and Se s and p orbitals for the highest occupied (N th) Bloch state at the Γ point, where N is electron filling. (b) zz shift vector component contributed by the Γ point. (c) Direct band gap at Γ as a function of strain. (d) Minimum direct band gap on the high-symmetry lines.

behavior also appears in the zxx and zyy components, a quantitative distinction exists between the zxx and zyy components, which can be proof of crystal axes. Last, the zyy component shows a maximum increase near the 4% strain for terahertz frequencies. It appears to be anomalous that the shift current exhibits a nonzero value at the limit where $\omega = 0$. On looking closely [see the inset of Fig. 4(d)], however, we find that the shift current response is smooth and well behaved at zero energy. Nonetheless, we believe that the abrupt sink in shift current could be experimental evidence of semimetallicity in the γ -GeSe system.

The abrupt change in shift current occurs near zero frequency in close conjugation with the near-zero-gap band inversion. The band inversion is featured in the orbital characters shown in Fig. 5(a). The Se (Ge) s + p -orbital character becomes dominant beyond 4% strain in the highest occupied (N th) Bloch state at Γ , where N is electron filling. Figure 5 shows that the band inversion significantly enhances the shift vector at Γ . We calculate the zz component of the shift vector $R_{nm}^{z,z} = \frac{\partial \phi_{nm}^z}{\partial k_z} + A_{nm}^z - A_{mm}^z$ [60], where A_{nm}^z is the z component of the Berry connection for the n th band and $\frac{\partial \phi_{nm}^z}{\partial k_z}$ is the phase of the z component of the interband transition dipole. This component of the shift vector is enhanced by 700%, from 5 to 35 \AA , via the band inversion. Thus, we speculate that the significant phase changes may accompany an orbital character

change induced by band inversion. This, in turn, could be responsible for an abrupt change in the shift current.

We attribute the origin of the considerable generation of shift current in γ -GeSe to the van der Waals layered geometry. As discussed for the band structure, DOS, and PDOS, the electronic structure of γ -GeSe consistently exhibits a quasi-two-dimensional (quasi-2D) nature, which can also be featured in the joint density of states. Similar to two-dimensional systems, in which the photovoltaic current is enhanced due to the large joint density of states [32,34], the layered geometry of γ -GeSe should play an essential role in generating a significant shift current. In this respect, van der Waals noncentrosymmetric systems are promising for generating a large shift current.

The shift current responses in these quasi-2D systems open exciting opportunities to study the dimensional crossover of shift current. The shift current along the out-of-plane direction is irrelevant in a genuine 2D system due to the vanishing shift vector responsible for the shift vector component. By contrast, γ -GeSe in quasi-two dimensions generates a significant shift current along the out-of-plane z direction. This observation motivates us to evaluate the shift vector components responsible for the z -directional shift current, such as the zz component. Our explicit calculations of the shift vector reveal that the magnitude of the zz component averaged over the whole BZ is ~ 0.407 \AA in the pristine layered γ -GeSe, while

it readily decreases to ~ 0.035 Å as we incorporate a 15 Å vacuum between the layers to suppress the interlayer coupling and mimic monolayer γ -GeSe. This calculation leads to the conclusion that, whereas the joint DOS has a 2D nature, a dimensional crossover has yet to dominate the shift vector in pristine γ -GeSe, leading to the enhancement of the shift current. Future studies should pin down the role of dimensionality in the generation of shift current. Still, our results already demonstrate that strained γ -GeSe is an intriguing test bed to study the dimensionality.

The enlarged shift vector via band inversion resembles that of topological phase transitions [39]. However, we point out that the exact topological phase transition is absent in this system within 5% strain. The absence of a topological phase transition is first reflected in the band gap as a function of strain, as shown in Figs. 5(c) and 5(d). A topological phase transition can occur via a band gap closer. However, the band gap remains open during the band inversion at Γ and the high-symmetry lines. The absence of a gap closer indicates that these systems are adiabatically connected and thus topologically equivalent. Furthermore, our explicit calculations indeed confirm that time-reversal \mathbb{Z}_2 invariants [52,53] and mirror Chern numbers [54,55] are all trivial, in line with the band gap change. Thus, we conclude that although the band inversion induces a significant change in the polarization as dictated in the shift vector, topological states remain the same within 5% uniaxial strain.

Finally, we point out that our calculations have a clear limitation bound to the single-particle approximation. Many-body effects can become prominent, in particular, in low-frequency regimes. We speculate that the Coulomb interaction may result in exciton binding between electrons and holes, enhancing the shift current response as in monolayer GeS [61] and monolayer MoS₂ [62]. In addition, the electron-phonon coupling may have a clear impact on shift current with sensitive dependence on the structural changes via strains, as demonstrated in

BaTiO₃ [63]. We believe these effects should be included for high-fidelity prediction.

IV. CONCLUSION

In conclusion, we have studied the shift current response of γ -GeSe under various uniaxial strains. We found a sensitive dependence of the shift current conductivity on the strain interplaying with the crystalline symmetries. Our calculations have demonstrated that shift current is tunable proof of various material properties. For example, meaningful information about the crystalline symmetries and thus the in-plane anisotropy can be proved by selectively measuring the shift current susceptibilities. More importantly, the shift current conductivity of γ -GeSe can inform the band gap. Experimentally, γ -GeSe was suggested as a low-gap semiconductor in Ref. [41]. However, their optical conductivity clearly showed the Drude peak in the direct current limit, which inarguably necessitates further explorations to pin down the electronic state. In this respect, our results should be useful. Encouragingly, a thin film of WSe₂ has been strained up to 7% using an atomic force microscope on SiO₂/Si substrates prepatterned with hole arrays [64]. Thus, we believe it is highly feasible to measure the abrupt increase of out-of-plane shift current upon the exertion of an in-plane slowly varying field, which could serve as an indicator of the semimetallic state of γ -GeSe.

ACKNOWLEDGMENTS

This work was supported by the Korean National Research Foundation (NRF) Basic Research Laboratory (Grant No. NRF-2020R1A4A3079707) and NRF Grant No. NRF-2021R1A2C1013871. The computational resources were provided by the Korea Institute of Science and Technology Information (KISTI; Grant No. KSC-2020-CRE-0108).

-
- [1] V. Fridkin, A. Grekov, A. Rodin, E. Savchenko, and T. Volk, Photoconductivity in ferroelectrics, *Ferroelectrics* **6**, 71 (1973).
 - [2] V. I. Belinicher and B. I. Sturman, The photogalvanic effect in media lacking a center of symmetry, *Sov. Phys. Usp.* **23**, 199 (1980).
 - [3] R. von Baltz and W. Kraut, Theory of the bulk photovoltaic effect in pure crystals, *Phys. Rev. B* **23**, 5590 (1981).
 - [4] D. Côté, N. v. Laman, and H. Van Driel, Rectification and shift currents in GaAs, *Appl. Phys. Lett.* **80**, 905 (2002).
 - [5] S. M. Young and A. M. Rappe, First Principles Calculation of the Shift Current Photovoltaic Effect in Ferroelectrics, *Phys. Rev. Lett.* **109**, 116601 (2012).
 - [6] D. Auston, A. Glass, and A. Ballman, Optical Rectification by Impurities in Polar Crystals, *Phys. Rev. Lett.* **28**, 897 (1972).
 - [7] A. Glass, D. Von der Linde, D. Auston, and T. Negran, Excited state polarization, bulk photovoltaic effect and the photorefractive effect in electrically polarized media, *J. Electron. Mater.* **4**, 915 (1975).
 - [8] W. Koch, R. Munser, W. Ruppel, and P. Würfel, Anomalous photovoltage in BaTiO₃, *Ferroelectrics* **13**, 305 (1976).
 - [9] B. M. Fregoso, Bulk photovoltaic effects in the presence of a static electric field, *Phys. Rev. B* **100**, 064301 (2019).
 - [10] F. Nastos and J. E. Sipe, Optical rectification and current injection in unbiased semiconductors, *Phys. Rev. B* **82**, 235204 (2010).
 - [11] S. M. Young, F. Zheng, and A. M. Rappe, First-Principles Calculation of the Bulk Photovoltaic Effect in Bismuth Ferrite, *Phys. Rev. Lett.* **109**, 236601 (2012).
 - [12] S. M. Young, F. Zheng, and A. M. Rappe, Prediction of a Linear Spin Bulk Photovoltaic Effect in Antiferromagnets, *Phys. Rev. Lett.* **110**, 057201 (2013).
 - [13] W. Shockley and H. J. Queisser, Detailed balance limit of efficiency of p-n junction solar cells, *J. Appl. Phys.* **32**, 510 (1961).
 - [14] A. Glass, D. v. d. Linde, and T. Negran, High-voltage bulk photovoltaic effect and the photorefractive process in LiNbO₃, in *Landmark Papers on Photorefractive Nonlinear Optics* (World Scientific, Singapore, 1995), pp. 371–373.
 - [15] V. Fridkin, Bulk photovoltaic effect in noncentrosymmetric crystals, *Crystallogr. Rep.* **46**, 654 (2001).

- [16] C. Somma, K. Reimann, C. Flytzanis, T. Elsaesser, and M. Woerner, High-Field Terahertz Bulk Photovoltaic Effect in Lithium Niobate, *Phys. Rev. Lett.* **112**, 146602 (2014).
- [17] L. Z. Tan, F. Zheng, S. M. Young, F. Wang, S. Liu, and A. M. Rappe, Shift current bulk photovoltaic effect in polar materials – Hybrid and oxide perovskites and beyond, *npj Comput. Mater.* **2**, 16026 (2016).
- [18] M. Bieler, K. Pierz, U. Siegner, and P. Dawson, Shift currents from symmetry reduction and coulomb effects in (110)-orientated GaAs/Al_{0.3}Ga_{0.7}As as quantum wells, *Phys. Rev. B* **76**, 161304(R) (2007).
- [19] M. Bieler, N. Laman, H. Van Driel, and A. L. Smirl, Ultrafast spin-polarized electrical currents injected in a strained zinc blende semiconductor by single color pulses, *Appl. Phys. Lett.* **86**, 061102 (2005).
- [20] X.-C. Zhang, Y. Jin, K. Yang, and L. J. Schowalter, Resonant Nonlinear Susceptibility near the GaAs Band Gap, *Phys. Rev. Lett.* **69**, 2303 (1992).
- [21] S. L. Chuang, S. Schmitt-Rink, B. I. Greene, P. N. Saeta, and A. F. J. Levi, Optical Rectification at Semiconductor Surfaces, *Phys. Rev. Lett.* **68**, 102 (1992).
- [22] N. Laman, M. Bieler, and H. Van Driel, Ultrafast shift and injection currents observed in wurtzite semiconductors via emitted terahertz radiation, *J. Appl. Phys.* **98**, 103507 (2005).
- [23] M. Sotome, M. Nakamura, J. Fujioka, M. Ogino, Y. Kaneko, T. Morimoto, Y. Zhang, M. Kawasaki, N. Nagaosa, Y. Tokura, and N. Ogawa, Spectral dynamics of shift current in ferroelectric semiconductor SbSi, *Proc. Natl. Acad. Sci. USA* **116**, 1929 (2019).
- [24] T. Ogden and D. Gookin, Bulk photovoltaic effect in polyvinylidene fluoride, *Appl. Phys. Lett.* **45**, 995 (1984).
- [25] R. K. Vijayaraghavan, S. C. Meskers, M. A. Rahim, and S. Das, Bulk photovoltaic effect in an organic polar crystal, *Chem. Commun.* **50**, 6530 (2014).
- [26] P. Král, E. J. Mele, and D. Tománek, Photogalvanic Effects in Heteropolar Nanotubes, *Phys. Rev. Lett.* **85**, 1512 (2000).
- [27] M. Ichiki, H. Furue, T. Kobayashi, R. Maeda, Y. Morikawa, T. Nakada, and K. Nonaka, Photovoltaic properties of (Pb, La)(Zr, Ti)O₃ films with different crystallographic orientations, *Appl. Phys. Lett.* **87**, 222903 (2005).
- [28] L. Pintilie, I. Vrejoiu, G. Le Rhun, and M. Alexe, Short-circuit photocurrent in epitaxial lead zirconate-titanate thin films, *J. Appl. Phys.* **101**, 064109 (2007).
- [29] M. Qin, K. Yao, and Y. C. Liang, High efficient photovoltaics in nanoscaled ferroelectric thin films, *Appl. Phys. Lett.* **93**, 122904 (2008).
- [30] L. Pintilie, V. Stancu, E. Vasile, and I. Pintilie, About the complex relation between short-circuit photocurrent, imprint and polarization in ferroelectric thin films, *J. Appl. Phys.* **107**, 114111 (2010).
- [31] M. Nakamura, F. Kagawa, T. Tanigaki, H. S. Park, T. Matsuda, D. Shindo, Y. Tokura, and M. Kawasaki, Spontaneous Polarization and Bulk Photovoltaic Effect Driven by Polar Discontinuity in LaFeO₃/SrTiO₃ Heterojunctions, *Phys. Rev. Lett.* **116**, 156801 (2016).
- [32] A. M. Cook, B. M. Fregoso, F. De Juan, S. Coh, and J. E. Moore, Design principles for shift current photovoltaics, *Nat. Commun.* **8**, 14176 (2017).
- [33] Y. Zhang, T. Holder, H. Ishizuka, F. de Juan, N. Nagaosa, C. Felser, and B. Yan, Switchable magnetic bulk photovoltaic effect in the two-dimensional magnet CrI₃, *Nat. Commun.* **10**, 3783 (2019).
- [34] T. Rangel, B. M. Fregoso, B. S. Mendoza, T. Morimoto, J. E. Moore, and J. B. Neaton, Large Bulk Photovoltaic Effect and Spontaneous Polarization of Single-Layer Monochalcogenides, *Phys. Rev. Lett.* **119**, 067402 (2017).
- [35] C. L. Kane, Topological band theory and the Z₂ invariant, in *Topological Insulators*, Contemporary Concepts of Condensed Matter Science Vol. 6 (Elsevier, Amsterdam, 2013), pp. 3–34.
- [36] A. Bansil, H. Lin, and T. Das, Colloquium: Topological band theory, *Rev. Mod. Phys.* **88**, 021004 (2016).
- [37] I. Sodemann and L. Fu, Quantum Nonlinear Hall Effect Induced by Berry Curvature Dipole in Time-Reversal Invariant Materials, *Phys. Rev. Lett.* **115**, 216806 (2015).
- [38] T. Morimoto and N. Nagaosa, Topological nature of nonlinear optical effects in solids, *Sci. Adv.* **2**, e1501524 (2016).
- [39] L. Z. Tan and A. M. Rappe, Enhancement of the Bulk Photovoltaic Effect in Topological Insulators, *Phys. Rev. Lett.* **116**, 237402 (2016).
- [40] J. Ahn, G.-Y. Guo, and N. Nagaosa, Low-Frequency Divergence and Quantum Geometry of the Bulk Photovoltaic Effect in Topological Semimetals, *Phys. Rev. X* **10**, 041041 (2020).
- [41] S. Lee, J.-E. Jung, H. gyu Kim, Y. Lee, J. M. Park, J. Jang, S. Yoon, A. Ghosh, M. Kim, J. Kim, W. Na, J. Kim, H. J. Choi, H. Cheong, and K. Kim, γ -GeSe: A new hexagonal polymorph from group IV–VI monochalcogenides, *Nano Lett.* **21**, 4305 (2021).
- [42] H.-G. Kim and H. J. Choi, Quasiparticle band structures, spontaneous polarization, and spin-splitting in noncentrosymmetric few-layer and bulk γ -GeSe, *J. Mater. Chem. C* **9**, 9683 (2021).
- [43] P. Giannozzi *et al.*, QUANTUM ESPRESSO: A modular and open-source software project for quantum simulations of materials, *J. Phys.: Condens. Matter* **21**, 395502 (2009).
- [44] M. J. van Setten, M. Giantomassi, E. Bousquet, M. J. Verstraete, D. R. Hamann, X. Gonze, and G.-M. Rignanese, The pseudodojo: Training and grading a 85 element optimized norm-conserving pseudopotential table, *Comput. Phys. Commun.* **226**, 39 (2018).
- [45] D. R. Hamann, Optimized norm-conserving Vanderbilt pseudopotentials, *Phys. Rev. B* **88**, 085117 (2013).
- [46] J. P. Perdew, K. Burke, and M. Ernzerhof, Generalized Gradient Approximation Made Simple, *Phys. Rev. Lett.* **77**, 3865 (1996).
- [47] H. J. Monkhorst and J. D. Pack, Special points for Brillouin-zone integrations, *Phys. Rev. B* **13**, 5188 (1976).
- [48] J. Ibañez-Azpiroz, S. S. Tsirkin, and I. Souza, *Ab initio* calculation of the shift photocurrent by Wannier interpolation, *Phys. Rev. B* **97**, 245143 (2018).
- [49] A. A. Mostofi, J. R. Yates, G. Pizzi, Y.-S. Lee, I. Souza, D. Vanderbilt, and N. Marzari, An updated version of wannier90: A tool for obtaining maximally-localised Wannier functions, *Comput. Phys. Commun.* **185**, 2309 (2014).
- [50] A. Damle and L. Lin, Disentanglement via entanglement: A unified method for Wannier localization, *Multiscale Model. Simul.* **16**, 1392 (2018).
- [51] V. Vitale, G. Pizzi, A. Marrazzo, J. R. Yates, N. Marzari, and A. A. Mostofi, Automated high-throughput Wannierisation, *npj Comput. Mater.* **6**, 66 (2020).
- [52] L. Fu, C. L. Kane, and E. J. Mele, Topological Insulators in Three Dimensions, *Phys. Rev. Lett.* **98**, 106803 (2007).

- [53] J. E. Moore and L. Balents, Topological invariants of time-reversal-invariant band structures, *Phys. Rev. B* **75**, 121306(R) (2007).
- [54] J. C. Y. Teo, L. Fu, and C. L. Kane, Surface states and topological invariants in three-dimensional topological insulators: Application to $\text{Bi}_{1-x}\text{Sb}_x$, *Phys. Rev. B* **78**, 045426 (2008).
- [55] T. H. Hsieh, H. Lin, J. Liu, W. Duan, A. Bansil, and L. Fu, Topological crystalline insulators in the SnTe material class, *Nat. Commun.* **3**, 982 (2012).
- [56] A. A. Soluyanov and D. Vanderbilt, Computing topological invariants without inversion symmetry, *Phys. Rev. B* **83**, 235401 (2011).
- [57] Q. Wu, S. Zhang, H.-F. Song, M. Troyer, and A. A. Soluyanov, Wanniertools: An open-source software package for novel topological materials, *Comput. Phys. Commun.* **224**, 405 (2018).
- [58] S. V. Gallego, J. Etxebarria, L. Elcoro, E. S. Tasci, and J. M. Perez-Mato, Automatic calculation of symmetry-adapted tensors in magnetic and non-magnetic materials: A new tool of the Bilbao crystallographic server, *Acta Crystallogr., Sect. A* **75**, 438 (2019).
- [59] R. Fei, L. Z. Tan, and A. M. Rappe, Shift-current bulk photovoltaic effect influenced by quasiparticle and exciton, *Phys. Rev. B* **101**, 045104 (2020).
- [60] B. M. Fregoso, T. Morimoto, and J. E. Moore, Quantitative relationship between polarization differences and the zone-averaged shift photocurrent, *Phys. Rev. B* **96**, 075421 (2017).
- [61] Y.-H. Chan, D. Y. Qiu, F. H. da Jornada, and S. G. Louie, Giant exciton-enhanced shift currents and direct current conduction with subbandgap photo excitations produced by many-electron interactions, *Proc. Natl. Acad. Sci. USA* **118**, e1906938118 (2021).
- [62] M. L. Trolle, G. Seifert, and T. G. Pedersen, Theory of excitonic second-harmonic generation in monolayer MoS_2 , *Phys. Rev. B* **89**, 235410 (2014).
- [63] Z. Dai, A. M. Schankler, L. Gao, L. Z. Tan, and A. M. Rappe, Phonon-Assisted Ballistic Current from First-Principles Calculations, *Phys. Rev. Lett.* **126**, 177403 (2021).
- [64] R. Zhang, V. Koutsos, and R. Cheung, Elastic properties of suspended multilayer WSe_2 , *Appl. Phys. Lett.* **108**, 042104 (2016).